Environ Earth Sci (2017) 76:17
DOI 10.1007/s12665-016-6310-1

ORIGINAL ARTICLE

Study of multi-aquifer groundwater interaction in a coal mining area in China using stable isotopes and major-ion chemical data

Pinghua Huang[1] · **Sumin Han**[2]

Received: 21 March 2016 / Accepted: 30 November 2016 / Published online: 22 December 2016

Abstract Investigations have been undertaken to determine the interactions between the main aquifers in a coal mining area near the Taihang Mountains in China to determine the sources of water. Environmental isotopes (^{18}O, ^{2}H, ^{3}H, ^{34}S) and water chemistry ions (Ca^{2+}, Mg^{2+}, Na^{+}, K^{+}, HCO_3^-, SO_4^{2-}, Cl^-) were used as tracers. Furthermore, batch sampling and testing were conducted on mountain spring water and karst water in the aquifers of the Taiyuan Group, Fengfeng Group, and Majiagou Group on the seatearth of the coal mining area, via field observations and laboratory experimental analysis. The $\delta^{18}O$ and $\delta^{2}H$ values of the mountain spring water and karst water in the coal mining area showed a common distribution with the local meteoric water line EL1 of karst water in the Majiagou Group but significantly deviated from the surface water evaporation line (EL2) in the coal mining area, when combined with the distribution of karst water level values. Thus, karst water in the coal mining area is mainly supplied by groundwater from mountainous areas. Furthermore, the concentration of sulfate ions increased dramatically in the groundwater flow of karst water from mountain spring water to karst water in the Fengfeng Group and Majiagou Group of the coal mining area. When equivalent concentrations of $(Ca^{2+} + Mg^{2+})/HCO_3^-$ and SO_4^{2-}/HCO_3^- reached their peak, the chemical type of groundwater gradually evolved from Ca–Mg–HCO_3 to Ca–Mg–SO_4–HCO_3. In addition, significant positive correlation was found between the $\delta^{34}S$ and SO_4^{2-} values of the water samples, indicating that gypsum is involved in groundwater lixiviation. In contrast, the relationships of Ca/Na versus Mg/Na, ($Na + HCO_3$) versus total dissolved solids (TDS), and Na^+ versus Cl^- revealed that TDS and salinity accumulate from the mountain spring water and karst water in the Taiyuan Group of the coal mining area. Furthermore, the chemical type of groundwater gradually evolved from Ca–Mg–HCO_3 to Na–HCO_3, as revealed by a Piper trilinear diagram.

Keywords Environmental isotopes · Karst water · Supply mechanism · Coal mining area

Introduction

With the gradual development of coal mining, the hydrogeological conditions of mines are becoming increasingly complex. Considering that deep groundwater is frequently encountered in coal mines, many explored coal resources have become difficult to exploit (Huang and Jian 2012). Therefore, understanding the groundwater flow dynamics in coal mining areas is important, and investigations that use hydrogeochemical methods to differentiate groundwater from different aquifers are important tools for achieving this goal.

Environmental isotopes have been used to trace regional groundwater movement, especially oxy-hydrogen stable isotopes, which themselves are part of water molecules (e.g., Tuttle et al. 2009; McArthur et al. 2001; Bouchaou et al. 2008; Wong and Clarke 2012; Layman et al. 2012). These isotopes can be used as conservative natural tracers with the ability to trace groundwater movements effectively (e.g., Clark and Fritz 1997; Jin et al. 2010;

✉ Pinghua Huang
hph2001@hpu.edu.cn

[1] Institute of Resources and Environment, Henan Polytechnic University, Jiaozuo 454000, China

[2] School of Electrical Engineering and Automation, Henan Polytechnic University, Jiaozuo 454000, China

Chapman et al. 2013; Atekwana and Seeger 2015; Otton et al. 2007; Parker et al. 2012; Scow and Hicks 2005; Su et al. 2012). To date, most research using stable isotopes as indicators of groundwater flow has focused on shallow aquifers, whereas relatively little work has been carried out using isotopes to characterize flow between series of deep aquifers; For example, Terwey (1984) used stable isotopes of oxygen and hydrogen to determine the likely sources of surface water and groundwater in arid and semiarid areas in Africa. The resultant isotopic data suggested that the White Nile is supplied by rainfall near the Equator of Central Africa, whereas the Blue Nile is supplied by rainfall in high-altitude regions of the Ethiopian Plateau. Furthermore, the water in both rivers is subject to the influence of evaporation; the groundwater and river water near the White Nile share similar isotopic signatures; groundwater is supplied by the nearest rainfall, whereas the groundwater near the Blue Nile is supplied in wet and cold climates. Criss and Davisson (1996) studied the relationship between agricultural irrigation water in Central California and overexploited groundwater. Analysis of oxygen isotopes suggested that the groundwater in the west of the valley is supplied not only by atmospheric precipitation but also by regional reinfiltration of agricultural irrigation water, whereas that in the east of the valley is supplied by drainage water from the Sierra Nevada. Tenalem et al. (2008) adopted environmental isotopes and other hydrochemical methods to study the relationship between surface water and groundwater in the Awash River Basin; they discussed the groundwater flow pattern based on the local geological background. Stable isotopes are commonly used in studies on the origin of groundwater and the altitude of recharge areas, and for determining the relative contribution of a number of water sources to groundwater recharge. Lima et al. (2003) used stable isotopes to determine the source of groundwater in the aquifer on the coastal plain of Recife, Brazil. Isotope analysis results indicated that the groundwater derived from three distinct water sources: recent groundwater recharge, delayed groundwater recharge that had been subject to evaporation, and saline water. Avner et al. (2007) studied the source of groundwater in the aquifer of the Israel Nubian Sandstone; the distinct isotopic composition suggested that groundwater was recharged from a variety of sources. Ahmed (2010) studied the variation of hydrogen and oxygen isotopes in groundwater between the Oman Gulf and Arabian Gulf, concluding that the groundwater was mainly recharged by rainfall whose water vapor came from the Mediterranean Sea. Furthermore, isotope data suggested that evaporation processes were involved in the rainfall recharge.

Stable isotope analysis also provides a convenient way to study the nature of interactions between surface water and groundwater, in coal-mining districts (Duan et al. 1994; Gui et al. 2005). Some scholars have carried out research to identify sources of groundwater inrush to mines in coal mining districts. In addition, based on water samples from this district, Feng and Guo (2003) established a neural network model for forecasting water inrush to mines via a backpropagation (BP) algorithm (a simple and popular method for updating the weights of networks) and artificial neural networks, the advantage of which is their ability to deal with nonlinear or unstructured problems. However, this method can only be used when water samples indicate clear differences in the hydrochemical components in groundwater from different aquifers. That analysis suggested that groundwater mixing occurred between aquifers. As a consequence of that work, investigation of the hydraulic connections between groundwater and surface water and the sources of groundwater recharge has become necessary to provide a scientific basis for groundwater safety assessment in coal mining districts.

The major aquifers of the study area have experienced many changes because of the effects of coal mining; significant changes have taken place in the groundwater seepage field. Hydraulic connections between local coal seams and aquifers have increased the difficulty of mining. In this study, isotope hydrogeochemical tracer techniques were used to investigate the hydrogeochemical characteristics of karst water in the Sihe coal mining area, as well as to reveal the characteristics of groundwater flow in the area. The objective of this study is to systematically explore the nature of groundwater interactions between aquifers and provide a firm basis for determining the sources of water inrush in this coal mining area.

Hydrogeological conditions

The Sihe coal mining area is located in the southeastern part of the Qinshui Basin. Its regional hydrogeological unit belongs to the Yanhe River Spring Basin with total area of 3000 km^2 (Fig. 1). The average flow of a single spring is 3.1 m^3/s; spring basin strata form a groundwater reservoir with the southern part sloping to the north and the eastern and western parts sloping to the center. Based on the flow field, two main groundwater flow directions exist, viz. from south to north, and from west to east. Underground karst water converges in the Sihe coal mining area, forming springs and seepages at the surface. Given the thick cover layer and poor runoff conditions, the Sihe coal mining area is considered a stagnation zone in the regional groundwater flow field.

The aquifers in the coal mining area can be divided as follows from top to bottom (Fig. 2): (1) the Quaternary pore aquifer composed of sands and gravels, with general thickness of 3–7 m and water inflow of 10–40 m^3/h; (2) the

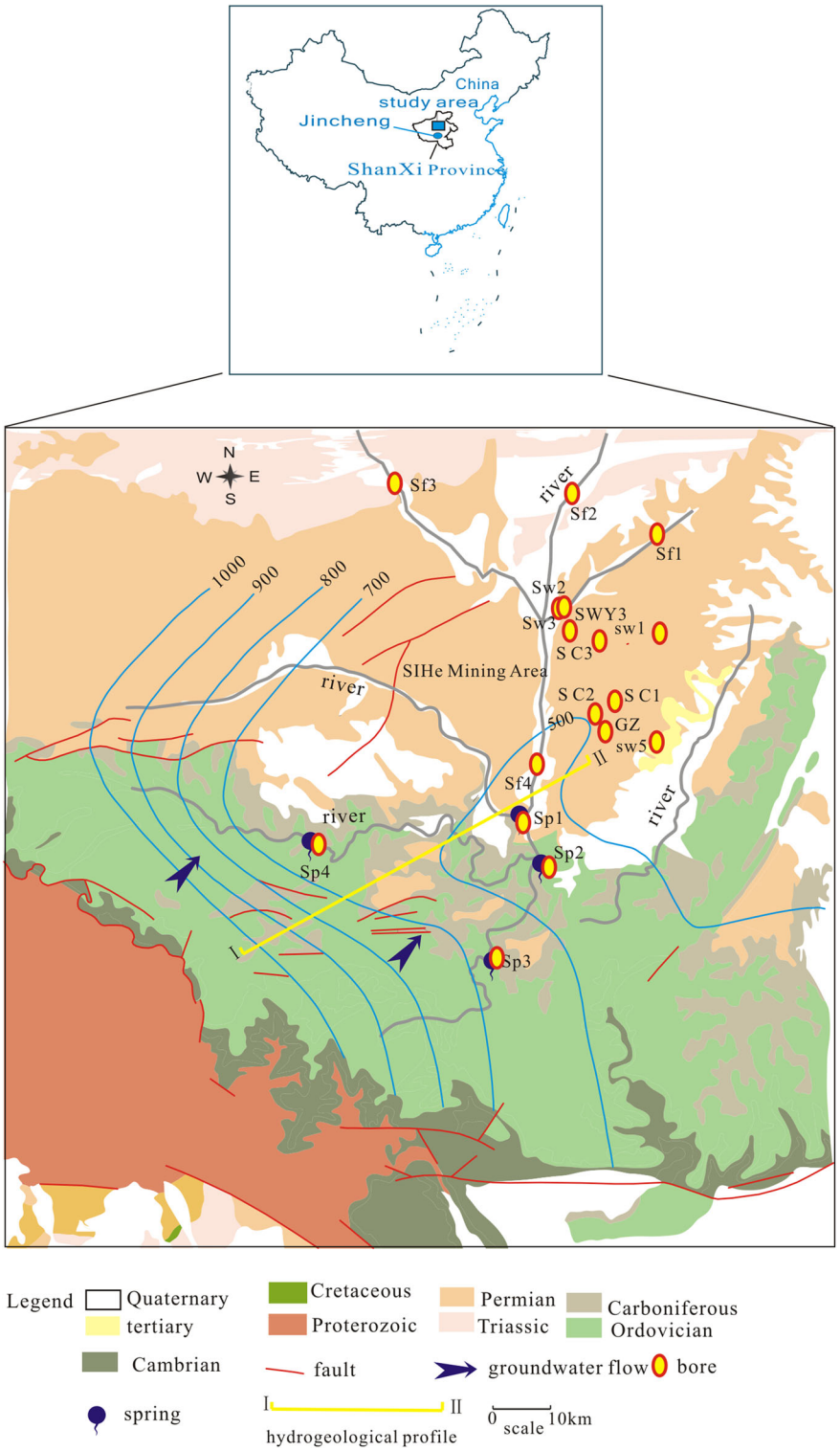

Fig. 1 Hydrogeological map of the Sihe coal mining district, China, with water sampling locations and karst water level contours (Majiagou Group limestone aquifer) indicated

Carboniferous carbonate aquifer, mainly referring to a thin layer of Carboniferous limestone fissure-karst water, generally containing significant water at burial depth of more than 25–30 m but only small amounts at burial depth of 5–10 m, with water inflow of 15–40 m^3/h; and (3) the Ordovician carbonate aquifer, which mainly develops in rock strata of the Fengfeng Group and Majiagou Group with large amounts of water, being the major aquifer of the carbonate aquifer group. Among these, the Fengfeng Group (O_{2f}), with depth of approximately 100 m, mainly

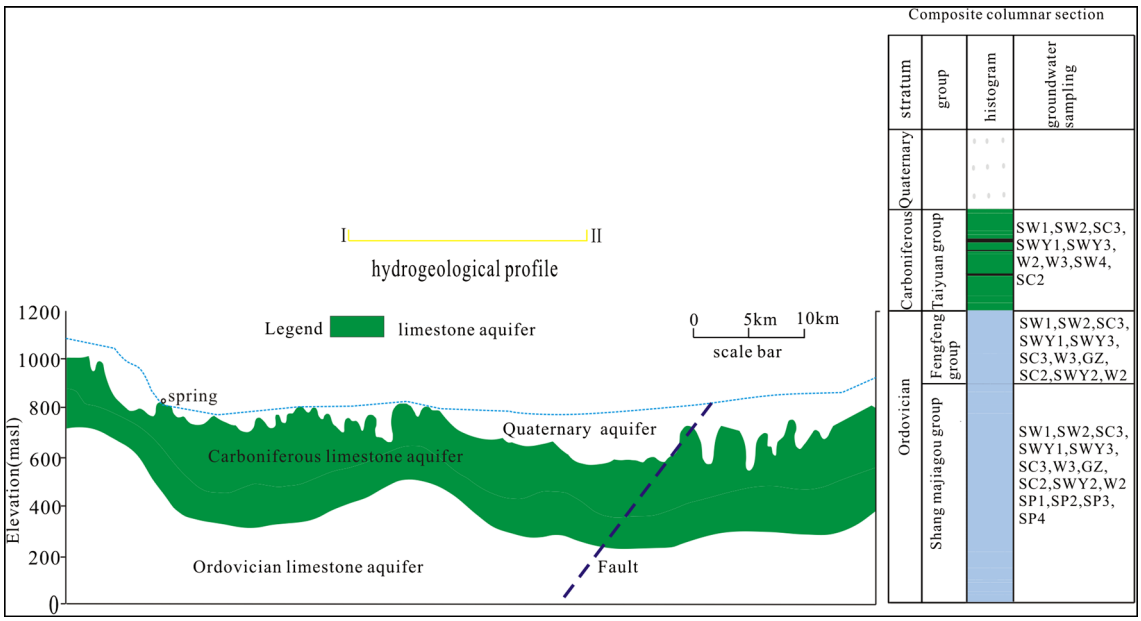

Fig. 2 Schematic cross-section, including hydrogeological profile and composite columnar section

comprises limestone, argillaceous limestone, and brecciated argillaceous limestone. The Majiagou Group (O_2s) with thickness of approximately 350 m mainly comprises dolomitic limestone, gray, and dark-gray limestone. The karst fissure is well developed and rich in water. Furthermore, dissolution phenomena, such as dissolved pores in general, may be observed.

The interfaces among all the aquifers are composed of aluminum mudstone, sandy mudstone, and other water-resistant layers; their thickness is generally 2–15 m, representing effective waterproof layers between aquifers.

Sample collection and testing

The water samples collected in the study area included spring water, river water, and groundwater from the coal mining area (Fig. 1). Groundwater was collected from the mining area. The electrical conductivity of water was measured in the field. Water samples were collected in clean plastic bottles (550 ml) for chemical analysis of major ions and stable isotopes. A total of 13 parameters were measured in all water samples, including TDS, pH, Ca^{2+}, Mg^{2+}, Na^{+}, K^{+}, HCO_3^{-}, SO_4^{2-}, Cl^{-}, $\delta^{18}O$, $\delta^{2}H$, $\delta^{3}H$, and $\delta^{34}S$. The results of these analyses together with eigenvalues are presented in Table 1. The hydrogen isotopes of water samples were measured by the zinc reaction method; oxygen isotopes were measured using the oxygen and carbon dioxide balance method with a MAT253 isotope mass spectrometer. The results are presented in comparison with the Vienna standard mean ocean water (VSMOW) standard, and the accuracies are ±0.2 and ±0.1‰, respectively. The content of radioactive tritium was measured by low-background liquid scintillation spectrometer (Tri-Carb 3170 TR/SL). The chemical composition of water samples was measured using a Shimadzu CTO-10ACvp ion chromatograph with relative error of 1%. Bicarbonate was measured by the dilute acid–methyl orange titration method.

Results and discussion

Hydrochemical analysis and discussion

The Piper trilinear diagram (Fig. 3) showed that groundwater in the study area could be mainly divided into the following three categories on the basis of differences in chemical composition: (1) Ca–Mg–HCO_3, (2) Na–HCO_3, and (3) Ca–Mg–SO_4–HCO_3.

Groundwater in the Taiyuan Group had chemical composition of predominantly Na–HCO_3, with cation concentration in the order $Na^{+} > Ca^{2+} > Mg^{2+}$ (Fig. 3), whereas that in the Fengfeng and Majiagou Groups was mainly Ca–Mg–SO_4–HCO_3. The chemical composition of mountain spring water was mainly Ca–Mg–HCO_3. Figure 3 shows how the chemical composition of groundwater changed with groundwater flow, and that water in the Sihe River in the mining area shared the same characteristics as the groundwater in the drainage area.

Table 1 Chemical and isotopic composition of water samples from the study area

Sample ID	Group	Na^+ (mmol/l)	K^+ (mmol/l)	Mg^{2+} (mmol/l)	Ca^{2+} (mmol/l)	F^- (mmol/l)	Cl^- (mmol/l)	SO_4^{2-} (mmol/l)	NO_3^- (mmol/l)
sf1	Surface water	0.3	0.1	0.7	6	0.1	0.2	2.2	0.4
sf2	Surface water	16.1	0.1	2	7.6	0.1	0.2	1	0.3
sf3	Surface water	1.2	0.1	1	2.9	0	0.4	1.2	0.6
sf4	Surface water	3.7	0.2	0.8	1.4	0	4.9	2.2	0.2
SWY1	Fengfeng Group	4.5	0	4	17.3		42.5	2.4	0.6
SWY3	Fengfeng Group	11.9	0	7.8	8.7		3.9	16.8	0.1
SWY2	Fengfeng Group	0.9	0	1.7	3.8		2.8	3.4	0.5
SW2	Fengfeng Group	21.2	0.1	7.4	14.8		11.9	24.8	0.1
w3	Fengfeng Group	16.3	0.6	1.7	5.9	0.1	0.8	2	0.2
SW1	Fengfeng Group	15	0.1	0.4	0.3		1.6	1.5	0.1
w2	Fengfeng Group	44.4	0.1	2.3	1	0.1	2.5	0.5	0.2
SC3	Fengfeng Group	7.6	0.1	0.5	0.8		0.9	3.7	0.6
GZ	Fengfeng Group	33.4	0.1	0.8	0.6		9.5	10.7	0.3
SC2	Fengfeng Group	10.9	0.1	0.6	0.5		5.5	2.6	0.4
sp1	Majiagou Group	0.5	0	1.7	2.9	0	0.4	1.4	0.4
sp2	Majiagou Group	0.7	0	1.1	2.3	0	0.4	1	0.4
sp3	Majiagou Group	0.6	0	1.5	3	0	3.2	1.9	0.4
sp4	Majiagou Group	0.8	0	1.4	2.5	0	0.5	1	0.4
sp5	Majiagou Group	8.3	0	1.6	2.2	0	0.4	1	0.2
sp6	Majiagou Group	8.1	0	1.5	2	0	0.6	1	0.2
sp7	Majiagou Group	8	0	1.6	3.3	0	0.6	2.3	0.3
sp8	Majiagou Group	8.5	0.1	1.5	2.8	0	0.6	2.2	0.3
SWY1	Majiagou Group	0.1	0.1	10.1	14.9		42	4.4	0.6
GZ	Majiagou Group	4.1	0.1	2.2	3.8		2.5	3.9	0.5
SC2	Majiagou Group	1.3	0.1	2.1	3.6		0.9	2.9	0.3
SC3	Majiagou Group	9.3	0.1	4.4	7.1		1.3	12.8	0.2
w2	Majiagou Group	10.6	0.1	7.7	16.8	0.1	3.2	11.3	0.1
w3	Majiagou Group	6.4	0.1	5.7	11.2	0.1	1.6	8.3	0.6
zl1	Majiagou Group	9.3	0.4	9.8	20	0.1	0.7	24	0.1
SW2	Majiagou Group	18.3	0.1	7.6	16.5		11.4	25.3	0.1
SWY2	Majiagou Group	2.2	0	1.1	4.9		1.1	5.6	0.5
SWY3	Majiagou Group	20	0.1	6.4	12.8		9.3	21.8	0.1
SW1	Majiagou Group	11	0.1	0.8	1.9		1.7	3.6	0.3
SW2	Taiyuan Group	14.4	0.1	0.4	0.1		4.8	1.4	0.5
SC3	Taiyuan Group	15.9	0.1	0.8	0.6		1.8	0.9	0.2
SW1	Taiyuan Group	14	0.1	0.4	0.2		1.7	1.2	0.1
SWY1	Taiyuan Group	16.3	0.1	0.2	0.1		1.4	0.8	0.1
SWY3	Taiyuan Group	13.2	0	0.6	0.3		1.5	1.2	0.4
w3	Taiyuan Group	27.8	0	0.1	0.2	0.2	1.9	1	0.2
w2	Taiyuan Group	15.2	0	0.1	0.2	0.3	1.9	2.4	0.1
SW4	Taiyuan Group	7.2	0.1	0.9	2.4		1.2	3.6	0.4
SC2	Taiyuan Group	16.4	0.1	0.2	0.3		9.6	2.3	0.2

Sample ID	Group	NO_2^- (mmol/l)	HCO_3^- (mmol/l)	CO_3^{2-} (mmol/l)	TDS (mg/l)	$\delta^{18}O$ (‰)	δD (‰)	H^3 (T.U.)	$\delta^{34}S$ (‰)
sf1	Surface water	0	5.4	1.5	928.6	−7.51	−55.1	4.05	
sf2	Surface water	0	29.4	1.6	2743.2	−3.75	−40.7	4.09	
sf3	Surface water	0.1	4.2	0	596.6	−7.24	−58.4	5.76	
sf4	Surface water	0	0.8	0	610.1	−6.56	−57.3	5.78	

Table 1 continued

Sample ID	Group	NO_2^- (mmol/l)	HCO_3^- (mmol/l)	CO_3^{2-} (mmol/l)	TDS (mg/l)	$\delta^{18}O$ (‰)	δD (‰)	H^3 (T.U.)	$\delta^{34}S$ (‰)
SWY1	Fengfeng Group	0	0.5	0	2694.9	−10.19	−80.1	1.05	17.39
SWY3	Fengfeng Group	0	5.7	0.9	2975.2	−10.64	−89.4	1.3	15.79
SWY2	Fengfeng Group	0	1.7	0	782.9	−11.49	−81.6	1.01	16.24
SW2	Fengfeng Group	0	4.1	0	4324.4	−10.92	−92.4	0.31	17.48
w3	Fengfeng Group	0	27.8	1.6	2511.4	−10.49	−83.8	2.44	18.39
SW1	Fengfeng Group	0	10	1	1250.8	−9.48	−83.6	2.15	16.21
w2	Fengfeng Group	0	43.8	1.5	4047.3	−11.89	−82.7	1.21	16.37
SC3	Fengfeng Group	0	1.3	0	731.8	−10.92	−95.4	0.61	18.94
GZ	Fengfeng Group	0	0.1	2.4	2341.2	−9.59	−82.8	2.54	17.98
SC2	Fengfeng Group	0	0.1	0.9	812.1	−11.28	−87.5	2.01	15.47
sp1	Majiagou Group	0	4.9	1.5	728.6	−9.05	−69.9	4.51	8.59
sp2	Majiagou Group	0	3.1	1.5	551.7	−9.07	−71.1	4.12	12.12
sp3	Majiagou Group	0	0.6	1.6	621.7	−9.21	−72.1	4.32	13.52
sp4	Majiagou Group	0	4.3	1.7	654.2	−11.8	−79.4	1.31	32.48
sp5	Majiagou Group	0	10	1.4	1140.7	−9.06	−69.1	5.07	7.12
sp6	Majiagou Group	0	8.8	1.6	1078.8	−8.41	−71.5	2.89	13.52
sp7	Majiagou Group	0	9	1.6	1260.4	−10.23	−69	4.45	9.89
sp8	Majiagou Group	0	8.3	1.7	1204	−10.75	−69.3	4.65	7.36
SWY1	Majiagou Group	0	0.2	0	2805.2	−11.89	−84	0.63	22.25
GZ	Majiagou Group	0	4.5	0.4	1095.1	−10.8	−77.4	1.48	18.98
SC2	Majiagou Group	0	5.6	0	902.7	−10.02	−72.2	2.54	17.25
SC3	Majiagou Group	0	4.9	0.3	2213.8	−11.69	−86	0.84	28.67
w2	Majiagou Group	0	30.8	1.5	4287.9	−11.8	−86.4	1.91	29.48
w3	Majiagou Group	0.1	18.5	1.4	2841.5	−9.22	−73.2	2.49	26.56
zl1	Majiagou Group	0	19.1	1.6	4870.9	−11.39	−86	0.54	33.17
SW2	Majiagou Group	0	4.7	0	4393.5	−10.8	−76.4	1.71	31.48
SWY2	Majiagou Group	0	1.2	0	962.7	−10.22	−73.2	2.94	24.15
SWY3	Majiagou Group	0	5	0.3	3887.1	−11.69	−84	0.67	29.67
SW1	Majiagou Group	0	6.3	0.5	1189.8	−10.92	−79.2	2.64	19.78
SW2	Taiyuan Group	0	0.1	1.2	761.6	−11.48	−89.6	1.51	15.89
SC3	Taiyuan Group	0	12	1.5	1400.1	−10.92	−79.4	1.34	16.12
SW1	Taiyuan Group	0	9.6	0.7	1149.5	−11.49	−85.8	1.67	14.69
SWY1	Taiyuan Group	0	10.8	1.6	1278.3	−10.49	−79.8	1.67	17.68
SWY3	Taiyuan Group	0	9.2	0.7	1131.9	−9.88	−76.6	1.05	14.32
w3	Taiyuan Group	0	20.5	1.5	2169.6	−10.09	−76.3	1.3	12.15
w2	Taiyuan Group	0	10.6	1.6	1417.5	−11.49	−81.6	1.01	15.43
SW4	Taiyuan Group	0	4.5	0.2	987.5	−9.49	−73.8	1.67	13.21
SC2	Taiyuan Group	0	0.1	1.2	1046.5	−10.49	−72.6	1.67	14.38

A two-dimensional coordinate graph (Fig. 4) showing the common logarithm of Moore ratios of groundwater hydrochemical data indicated significant ($R = 0.88$) correlation between Ca/Na and Mg/Na. This correlation reflects similar formation mechanisms of Ca, Mg, and Na in the groundwater, thereby suggesting that the lithology of aquifer medium significantly affects how the chemical composition of groundwater evolves in the area. Incongruent dissolution of carbonate likely exerts strong control on the chemical composition of groundwater via the following reaction:

$$x\mathrm{CaMg}(\mathrm{CO_3})_2 + 2x\mathrm{H_2O} + 2x\mathrm{CO_2(g)} = x\mathrm{Ca^{2+}} + 4x\mathrm{HCO_3^-} + x\mathrm{Mg^{2+}} \quad (1)$$

Figure 5 shows that, in the direction of groundwater flow (from the mountain spring water to the karst water of Taiyuan Group), the TDS, Na^+, and Cl^- values progressively increased while the chemical composition changed

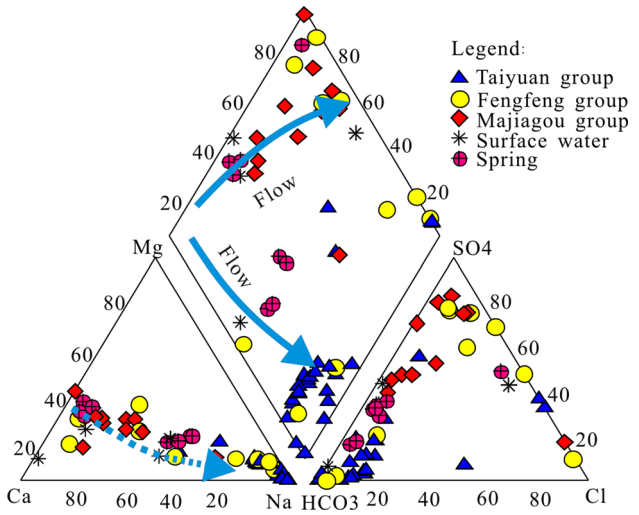

Fig. 3 Piper trilinear diagram for major ions in water from Sihe coal mining district. Data from Table 1

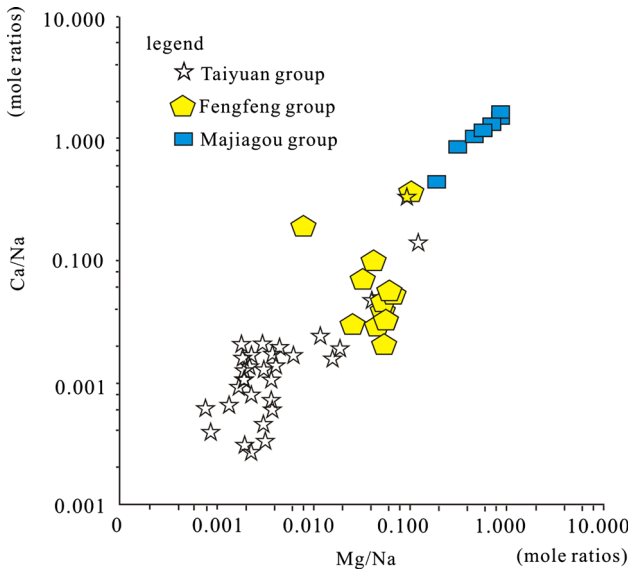

Fig. 4 Coordinate graph with common logarithm of mole ratios of groundwater hydrochemical data between Ca/Na and Mg/Na (the mole ratio is the ratio of the number of moles of calcium or magnesium ions, respectively, to sodium ions per unit volume)

from Ca–Mg–HCO_3 to Na–HCO_3. Rocksalt dissolution and cation exchange (Ca^{2+}–Na^{+}, Mg^{2+}–Na^{+}) are likely the major hydrochemical mechanisms responsible for these changes. Cation exchange associated with silty sediments in the Taiyuan Group is also likely to affect the cationic composition of groundwater via the following reactions:

$$2Na^{+}(\text{rock}) + Ca^{2+}(\text{water}) = 2Na^{+}(\text{water}) + Ca^{2+}(\text{rock}) \quad (2)$$

$$2Na^{+}(\text{rock}) + Mg^{2+}(\text{water}) = 2Na^{+}(\text{water}) + Mg^{2+}(\text{rock}) \quad (3)$$

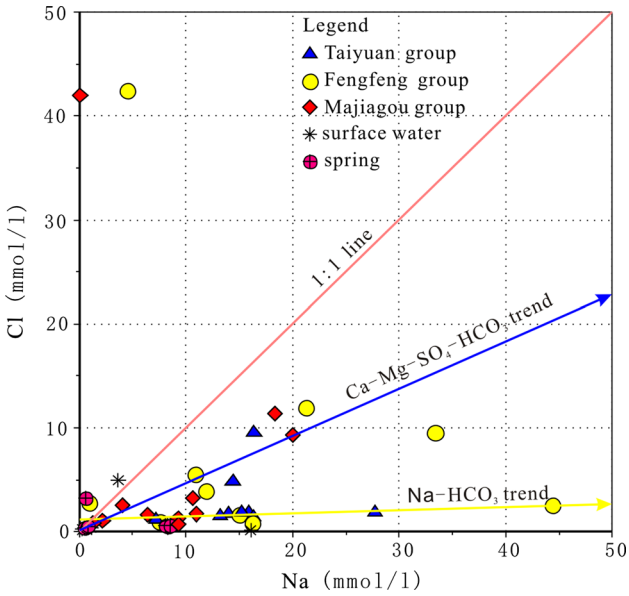

Fig. 5 Cl^{-} versus Na^{+} of water samples from the study area

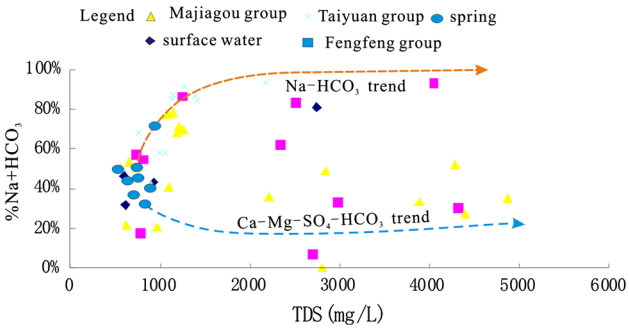

Fig. 6 %(Na + HCO_3) versus TDS of water samples from the study area

As the TDS increased gradually from the mountain spring water to the karst water of the Fengfeng and Majiagou Groups, the chemical composition of the groundwater gradually changed from Ca–Mg–HCO_3 to Ca–Mg–SO_4–HCO_3 (Fig. 6). Furthermore, the concentration of sulfate ions increased sharply. Figure 7 shows that the equivalent concentration ratios of $(Ca^{2+} + Mg^{2+})/HCO_3^{-}$ and SO_4^{2-}/HCO_3 of the Fengfeng and Majiagou Groups in the coal mining area plateau at a maximum value, thereby suggesting that gypsum dissolution exerts significant control on groundwater composition via the following reaction:

$$Ca_xMg_{1-x}SO_4 \cdot 2H_2O = xCa^{2+} + (1-x)Mg^{2+} + SO_4^{2-} + 2H_2O \quad (4)$$

Also described is the sulfuric acid participation in carbonate dissolution in the chemical reaction equations. The value of $(Ca^{2+} + Mg^{2+})/HCO_3^{-}$ gradually decreases with

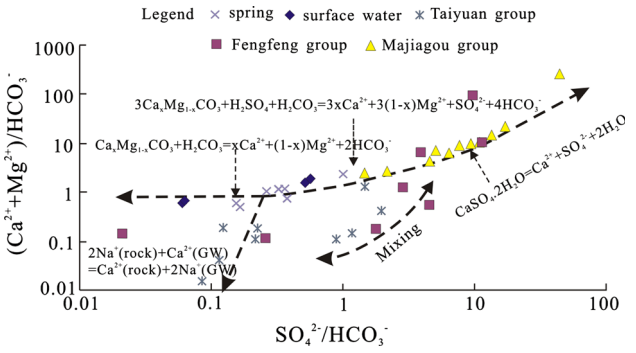

Fig. 7 $(Ca^{2+} + Mg^{2+})/HCO_3^-$ versus SO_4^{2-}/HCO_3^- of water samples from the study area (meq:meq)

the same value of SO_4^{2-}/HCO_3^- and cation exchange occurring. The water samples with low SO_4^{2-}/HCO_3^- ratio show that dissolution of carbonate rock mainly occurs. With increasing ratios of $(Ca^{2+} + Mg^{2+})/HCO_3^-$ and SO_4^{2-}/HCO_3^-, gypsum dissolves.

Isotope analysis and discussion

Analyzing the relationship between the isotopes ^{18}O and ^{2}H in groundwater and rainfall allows determination of the factors that influence groundwater recharge. In arid and semiarid regions, the global meteoric water line (GMWL) serves as a baseline for estimating factors that influence the geochemical evolution of groundwater. Accordingly, this study used the global meteoric water line (GMWL) ($\delta^2H = \delta^{18}O + 10$) as reference. Figure 8 shows that the ($\delta^{18}O$, δ^2H) points for the mountain spring water and the karst water (including the Taiyuan, Fengfeng, and Majiagou Groups) in the coal mining area lie in the same region, mostly below the GMWL. The ($\delta^{18}O$, δ^2H) points of spring water and groundwater are distributed along the same evaporation line (EL1, obtained from fitting to the

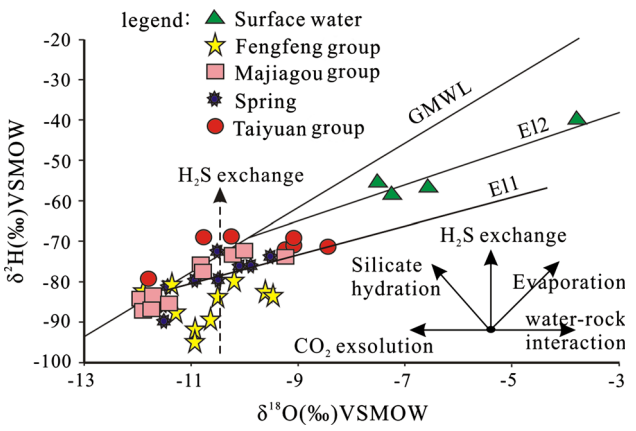

Fig. 8 δ^2H versus $\delta^{18}O$ plot of stable isotope composition of water from the study area, indicating the recharge sources of groundwater. The global meteoric water line (GMWL) is $\delta^2H = 8 \times \delta^{18}O + 10$

samples of karst water in the Majiagou Group). During the process of rainfall infiltration, ^{18}O and ^{2}H in the water will be enriched because of evaporation or interaction between rocks and water. If groundwater comes from local precipitation, EL1 should coincide with EL2 (the fitting line for local surface water samples) or be located above EL2. In Fig. 8, the difference between the groundwater evaporation line (EL1) and surface water evaporation line (EL2) indicates that local precipitation and surface water are not the main sources of groundwater recharge. Given the common distribution of karst water with EL1, groundwater is subjected to evaporation to different degrees before the source infiltrates underground. This phenomenon suggests that karst water mainly comes from groundwater in mountainous areas. A few spring water samples fell on the GMWL, indicating that they are directly supplied by rainfall infiltration. The ($\delta^{18}O$, δ^2H) points for some samples were nearly distributed along the GMWL, with some lying slightly above or below. This observation indicates that some of the supplemental water is lost because of silicate hydrolysis or evaporation.

From the Taiyuan Group, Fengfeng Group, to Majiagou Group in the Sihe mining area, the δ^2H, $\delta^{18}O$, TDS, and Cl^- values for karst water of aquifers decreased, whereas the $\delta^{34}S$ and SO_4^{2-} values gradually increased. This result indicates that the vertical hydraulic connection between aquifers is rather weak, with lateral runoff dominating in the groundwater. Figure 8 shows that the distribution of karst water samples in the Fengfeng Group tended to be vertical, indicating that ^{2}H of karst water in this layer has drifted. This movement may be the result of exchange via H_2S. The closed deposition environment enables anaerobic bacteria to stimulate reduction of sulfate, generating high H_2S (high solubility of H_2S can be tested at the drilling hole on site). The exchange reaction of hydrogen isotopes is $H_2O + HDS = HDO + H_2S$. Consequently, an exchange equilibrium reaction of hydrogen isotopes occurs.

Sulfur isotopes are stable under the chemical conditions present in aquifers in the study area, enabling their use as

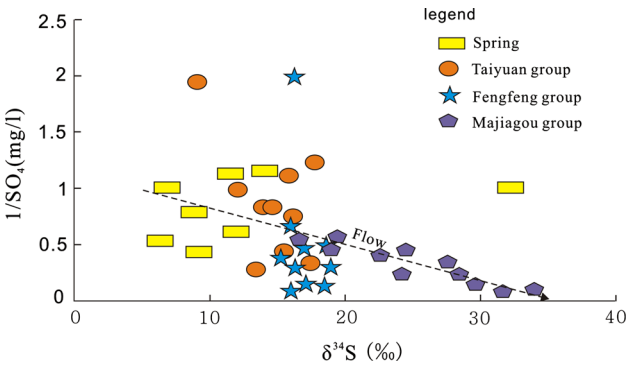

Fig. 9 $1/SO_4$–$\delta^{34}S$ plot of the ^{34}S isotope composition of water in the study area, indicating the ^{34}S sources of groundwater

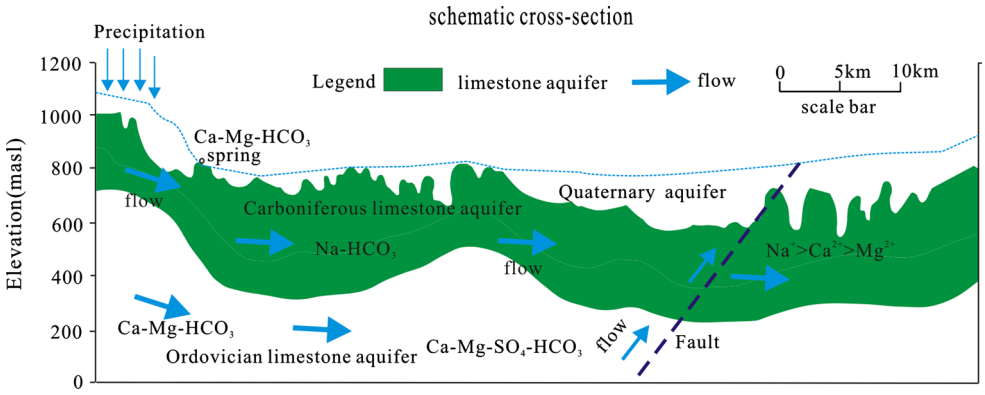

Fig. 10 Conceptual model of groundwater flow paths in the study area, showing groundwater flow paths and recharge sources that influence groundwater quality in the region

tracers for sources of sulfate ions in karst water. Furthermore, the major sources of sulfate in groundwater are as follows: dissolution of evaporites (e.g., gypsum), oxidation of sulfides (mainly including pyrite), dry and wet deposition from atmosphere, application of chemical fertilizers, infiltration of industrial and mining wastewater, acid precipitation, etc. During open hydrological circulation, dissolution of gypsum and oxidation of sulfides will result in fractionation of the sulfur isotopes in sulfate, resulting in changes of the sulfur isotopes. In the closed sedimentary environment, anaerobic bacteria will promote reduction of sulfate ions; light ^{32}S will initially react, while heavy ^{34}S will gather in the residual sulfate.

The concentration of SO_4^{2-} in the karst water of the Majiagou Group in the coal mining area ranged from 322.4 to 1926 mg/l, whereas that for Taiyuan Group was relatively low, ranging from 11.0 to 147.4 mg/l; furthermore, the range of $\delta^{34}S$ was also larger, from 2.08 to 10.20‰ (average 3.83‰). Figure 9 shows that the $\delta^{34}S$ value of SO_4^{2-} in the karst water of the Majiagou Group was extremely high. Furthermore, the $\delta^{34}S$–SO_4^{2-} relationship reveals that $\delta^{34}S$ and SO_4^{2-} in water show a significant positive correlation, indicating that sulfate in karst water is affected by dissolution of gypsum. $\delta^{34}S$ in the stagnation region is obviously higher than in the recharge area, indicating that the stagnation time of karst water is long and the circulation is deep. No obvious correlation was found between the concentration of SO_4^{2-} and the value of $\delta^{34}S$ in the karst water of the Taiyuan Group. Furthermore, the concentration changes of SO_4^{2-} ions are larger, and the values of $\delta^{34}S$ are also divergent, indicating many sources of SO_4^{2-}.

Conclusions

The mechanism of evolution of groundwater quality and flow can be described based on the conceptual model shown in Fig. 10. Ordovician limestone groundwater, Carboniferous limestone groundwater, and Quaternary groundwater have a tendency to increase gradually from the Taihang Mountains areas to the coal mining district, indicating accumulation of ions along the groundwater flow path. The bare Ordovician limestone stratum in the foothills of the Taihang Mountains receives precipitation recharge, forming karst water of Ca–Mg–HCO_3 type. Strong leakage zones may exist in the bare Ordovician limestone of the mountainous area. During the supply process of groundwater flow, cation-exchange adsorption, carbonate filtration, and gypsum dissolution play key roles in the hydrochemical evolution of groundwater.

Thorough application of the δ^2H–$\delta^{18}O$ relationship, SO_4^{2-}–$\delta^{34}S$ relationship, ^3H isogram, Piper trilinear diagram, ion ratio, and other similar methods not only enables investigation of the runoff mechanism of groundwater recharge in the coal mining area but can also reasonably identify the groundwater of the Taiyuan Group, Fengfeng Group, and Majiagou Group. The $\delta^{18}O$, δ^2H, ^3H, and $\delta^{34}S$ characteristics of the groundwater in the study region reveal that the karst water (including the Taiyuan Group, Fengfeng Group, and Majiagou Group) in the Sihe coal mining area is supplied by groundwater coming from high-altitude mountainous areas. The vertical hydraulic relationship between aquifers of the Taiyuan Group, Fengfeng Group, and Majiagou Group in the coal mining area is rather weak. Furthermore, lateral runoff dominates in the karst water. The results of this study provide an accurate theoretical basis to infer the sources of water inrush in this coal mining area.

Acknowledgements This work was financially supported by the Science and Technology Key Research Project of the Education Department of Henan, China (nos. 13A170313, 14A510022) and the Technological Innovation Team of Colleges and Universities in Henan, China (Grant 15IRTSTHN027).

References

Ahmed M (2010) Evolution of isotopic compositions in groundwater of the area between the Gulf of Oman and the Arabian Gulf. Chin J Geochem 29:152–156

Atekwana EA, Seeger EJ (2015) Carbonate and carbon isotopic evolution of groundwater contaminated by produced water brine with hydrocarbons. Appl Geochem 63(12):105–115

Avner V, Sharona H, Jiwchar G et al (2007) New isotopic evidence for the origin of groundwater from the Nubian Sandstone Aquifer in the Negev, Israel. Appl Geochem 22:1052–1073

Bouchaou L, Michelot JL, Vengosh A, Hsissou Y, Qurtobi M, Gaye CB, Bullen TD, Zuppi GM (2008) Application of multiple isotopic and geochemical tracers for investigation of recharge, salinization, and residence time of water in the Souss-Massa aquifer, southwest of Morocco. J Hydrol 352:267–287

Chapman EC, Capo RC, Stewart BW, Hedin RS, Weaver TJ, Edenborn WM (2013) Strontium isotope quantification of siderite, brine and acid mine drainage contributions to abandoned gas well discharges in the Appalachian Plateau. Appl Geochem 31:109–118

Clark ID, Fritz P (1997) Environmental isotopes in hydrogeology. Lewis, Boca Raton

Criss RE, Davisson ML (1996) Isotopic imaging of surface water/groundwater interactions, Sacramento Valley, California. J Hydrol 178:205–222

Duan YC, Hei L, Xie GX (1994) Application of environmental isotopes in the drain test of Xingtai Mine. Coal Geol Explor 22(1):33–37 **(in Chinese)**

Feng LJ, Guo XS (2003) The application of artificial neural network theory to mine water inrush prediction. J Xi'an Univ Sci Technol 23(4):369–371 **(in Chinese)**

Gui HR, Chen LW, Song XM (2005) Features of oxygen and hydrogen stable isotopes in deep groundwater in mining area of northern Anhui. J Harbin Inst Technol 37(1):111–114

Huang PH, Jian SC (2012) Recharge sources and hydrogeochemical evolution of groundwater in the coal-mining district of Jiaozuo, China. Hydrogeol J 20:739–754

Jin L, Siegel DI, Lautz LK, Mitchell MJ, Dahms DE, Mayer B (2010) Calcite precipitation driven by the common ion effect during groundwater surface-water mixing: a potentially common process in streams with geologic settings containing gypsum. Geol Soc Am Bull 122(7–8):1027–1038

Layman CA, Araujo MS, Boucek R, Hammerschlag-Peyer CM, Harrison E, Jud ZR, Matich P, Rosenblatt AE, Vaudo JJ, Yeager LA, Post DM, Bearhop S (2012) Applying stable isotopes to examine food-web structure: an overview of analytical tools. Biol Rev 87:545–562

Lima ES, Montenegro SMG, Montenegro AA (2003) Environmental isotopes and the analysis of the origin of groundwater salinity in the Cabo aquifer in Recife coastal plain, Pernambuco, Brazil. Short papers–IV South American Symposium on Isotope Geology

McArthur JM, Howarth RJ, Bailey TR (2001) Strontium isotope stratigraphy; LOWESS Version 3; best fit to the marine Sr-isotope curve for 0–509 Ma and accompanying look-up table for deriving numerical age. J Geol 109:155–170

Otton JK, Zielinski RA, Smith BD, Abbott MM (2007) Geologic controls on movement of produced-water releases at US Geological Survey Research Site A, Skiatook Lake, Osage county, Oklahoma. Appl Geochem 22(10):2138–2154

Parker SR, Gammons CH, Smith MG, Poulson SR (2012) Behavior of stable isotopes of dissolved oxygen, dissolved inorganic carbon and nitrate in groundwater at a former wood treatment facility containing hydrocarbon contamination. Appl Geochem 27(6):1101–1110

Scow KM, Hicks KA (2005) Natural attenuation and enhanced bioremediation of organic contaminants in groundwater. Curr Opin Biotechnol 16(3):246–253

Su XS, Lv H, Zhang WJ, Zhang YL, Xiao J (2012) Evaluation of petroleum hydrocarbon biodegradation in shallow groundwater by hydrogeochemical indicators and C, S-isotopes. Environ Earth Sci 69(6):2091–2101

Tenalem A, Seifu K, Tamiru A (2008) Environmental isotopes and hydrochemical study applied to surface water and groundwater interaction in the Awash River basin. Hydrol Process 22:1548–1563

Terwey JL (1984) Isotopes in groundwater hydrology, challenges in African hydrology and water resources. IAHS Publ 144:155–160

Tuttle MLW, Breit GN, Cozzarelli IM (2009) Processes affecting $d^{34}S$ and $d^{18}O$ values of dissolved sulfate in alluvium along the Canadian River, central Oklahoma, USA. Chem Geol 265:455–467

Wong WW, Clarke LL (2012) A hydrogen gas–water equilibration method produces accurate and precise stable hydrogen isotope ratio measurements in nutrition studies. J Nutr 142:2057–2062